Flexibility Does Not Change the Polarizability of Water Molecules in the Liquid

Bernhard Schropp and Paul Tavan*

Lehrstuhl für Biomolekulare Optik, Ludwig-Maximilians-Universität, Oettingenstr. 67, 80538 München, Germany

Received: November 17, 2009; Revised Manuscript Received: December 18, 2009

Molecular mechanics (MM) force fields employed in molecular dynamics simulations of bulk liquid water or of solvated proteins have to appropriately handle the sizable polarizability α of the water molecules. Using a hybrid method that combines density functional theory (DFT) for a rigid water molecule with an MM description of the liquid environment, we have recently shown that the induced dipole moment can be accurately calculated by linear response multiplying the experimental gas phase polarizability α^{exp} with the electric reaction field averaged over the volume of the molecule [B. Schropp and P. Tavan, *J. Phys. Chem. B* **2008**, *112*, 6233]. However, water molecules are flexible, and the strong local fields acting in the liquid can change their geometries. These changes of geometry can modify both the dipole moment and the polarizability. Using a DFT/MM approach for a flexible DFT water model, here we show that the corresponding effects are quite small. Moreover, they even happen to cancel. As a result, rigid, transferable, and polarizable MM models automatically include the couplings between the external field in the bulk liquid, the geometry, and the dipole moment of an embedded water molecule.

1. Introduction

Computer simulations of biological processes at the molecular level depend not only on the correct description of the acting biomolecules but also on that of the environment.[1,2] Typically, this environment consists of liquid water at ambient temperature and pressure. Therefore, the correct modeling of the water is of key importance.

Approaches aiming at a description of liquid water range from continuum methods representing the most coarse grained view,[3,4] over simple atomistic three-point water models,[5,6] and more sophisticated models[7,8] up to so-called first-principles techniques enabling simulations of small periodic water boxes.[9,10] The multitude of suggested approaches is a consequence of the well-known conflict between accuracy and efficiency generally characteristic for numerical modeling. Correspondingly, the choice of a specific approach is application dependent.

For accurate descriptions of large molecules in solution, explicit and atomistic descriptions of the aqueous environment cannot be avoided up to now.[2,11−14] In simulation systems adequate for solvated proteins, the water atoms should outnumber the protein atoms by at least a factor of 10.[15] Correspondingly, in a recent 10 μs folding simulation of a small protein in water, this factor was about 60.[16] Thus, 98% of the computation time required by this huge simulation had to be spent on describing the thermal motion of the aqueous solvent although its properties were by no means in the focus of this study.

Molecular Mechanics Water Models. Thus, reasons of computational manageability suggest for biomolecular simulations the use of very simple mechanical water models. Such models typically use the three atomic sites within the water molecule (cf. Figure 1) for a description of its interactions with other molecules. The atomic sites carry the nuclear masses and certain partial charges generating Coulomb interactions. These charges are chosen to reproduce the average dipole moments of the water molecules in the bulk liquid thus accounting for the large induced dipole moments. The Pauli repulsion and the dispersion interaction are described by Lennard−Jones potentials. Most models fix the molecular geometry $\mathbf{G} \equiv \{\varphi_{HOH}, r_{OH,1}, r_{OH,2}\}$ at predefined values of φ_{HOH} and $r_{OH,1} = r_{OH,2}$.

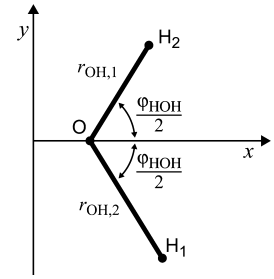

Figure 1. Geometry of the water molecule and the coordinate system employed for its description.

Water molecules are highly polarizable. Therefore, transferring simple models from the bulk liquid into other environments like the surface or the interior of a protein quickly deteriorates the model quality. A recent computational study[17] has demonstrated, for instance, that the dipole moments of the three crystallographic water molecules in the chromophore binding pocket of bacteriorhodopsin are 10% larger than in the bulk liquid. Findings like the latter suggest that it may be necessary to include an explicit description of the electronic polarizability in water models employed in biomolecular simulations despite the correspondingly increased computational effort.

Addressing this issue, a multitude of polarizable water models were previously suggested (for recent reviews, see refs 18−20). Many of them proposed to extend the simple models by adding inducible dipoles[21−28] or so-called Drude oscillators.[29−34] All these approaches have to choose a value for the polarizability α that enters a linear response relation $\boldsymbol{\mu}^i = \alpha \mathbf{E}(\mathbf{r}_\mu)$ for the induced dipole moment $\boldsymbol{\mu}^i$. Here the polarizing electric field $\mathbf{E}$

* Corresponding author. E-mail: tavan@physik.uni-muenchen.de. Phone: +49-89-2180-9220.

10.1021/jp910932b
Published on Web 01/20/2010

is measured at a predefined site $\mathbf{r}_\mu$ (e.g., the position $\mathbf{r}_O$ of the oxygen atom) within the water molecule.

Inhomogeneity of the Local Reaction Fields. Quantum mechanically, however, it is not the field at a specific site within the molecule which generates the induced dipole moment μ^i, but instead an average $\langle \mathbf{E} \rangle_v$ of the field $\mathbf{E}(\mathbf{r})$ over the molecular volume v. In the presence of field inhomogeneities, the average $\langle \mathbf{E} \rangle_v$ may differ from a spot check $\mathbf{E}(\mathbf{r}_\mu)$. As recently shown by us, in the bulk liquid these inhomogeneities are very large.[35] As a result, the spot check $\mathbf{E}_O \equiv \mathbf{E}(\mathbf{r}_O)$ overestimates the polarizing field $\langle \mathbf{E} \rangle_v$ on average by 46%. In polarizable molecular mechanics (MM) models for water, in which one has to use a spot check like $\mathbf{E}_O$ for measuring the polarizing field, one can approximately correct this systematic error by estimating the polarizing field as $\langle \mathbf{E} \rangle_v \approx 0.684\mathbf{E}_O$. As a parameter of linear response, one should then employ the experimental[36] gas phase polarizability $\alpha^{exp} = 1.47$ Å^3.

The quoted result was obtained by the following computational approach. First, the molecular dynamics (MD) of a periodic box filled with MM water models was simulated at room temperature and ambient pressure to generate an equilibrium ensemble of water configurations. From each configuration, one of the molecules was selected for a treatment by density functional theory (DFT), while the MM description was retained for the remainder. The polarizing field generated by the environment of the selected molecule was imported into its DFT Hamiltonian.[37] Its geometric parameters were kept fixed at the experimental gas phase values,[38] and its dipole moment was calculated by DFT. The DFT/MM-MD data obtained for the induced dipole moments were reproduced by the linear response relation $\boldsymbol{\mu}^i = \alpha \langle \mathbf{E} \rangle_v$ with a standard deviation of only 0.02 D, where α is the polarizability of the isolated DFT water model.

Effects of Flexibility. According to the Boltzmann distribution, in the liquid phase and at physiological temperatures the vibrational modes of nearly all water molecules are frozen in the vibrational ground states. Here, the molecules are neither rigid nor classical harmonic oscillators, and their equilibrium geometry depends on the external field. To include the latter effect into MM−MD simulations, flexible constraints should be applied to the geometries of the water molecules.[39,40] Fortunately, the correspondingly increased computational effort can be avoided because the accuracy losses become very small, if the molecular geometry $\mathbf{G}$ is rigidly constrained to a suitably chosen average $\langle \mathbf{G} \rangle$.[41] In view of these results, our previous decision of choosing the experimental gas phase geometry $\mathbf{G}^g$ for evaluating induced dipole moments may have been suboptimal.

Because we had rigidly fixed our water models to $\mathbf{G}^g$, our preceding study focused on the effects which are caused by the polarization of the electron density within the DFT fragment at this geometry.[35] However, when exposed to an external field $\mathbf{E}(\mathbf{r})$, which we will represent from now on by the volume average electric field $\langle \mathbf{E} \rangle_v$, a water molecule will also change its geometry $\mathbf{G}$ and thereby indirectly its electrostatic properties $\boldsymbol{\mu}$ and α. The direct and indirect changes of the dipole moment $\boldsymbol{\mu}$ may be represented by the modified response relation

$$\boldsymbol{\mu} = \boldsymbol{\mu}^g + \Delta\boldsymbol{\mu}^g[\mathbf{G}(\langle \mathbf{E} \rangle_v)] + \{\alpha_e + \Delta\alpha_e[\mathbf{G}(\langle \mathbf{E} \rangle_v)]\}\langle \mathbf{E} \rangle_v \quad (1)$$

where $\boldsymbol{\mu}^g$ is the dipole moment of an isolated water molecule; $\Delta\boldsymbol{\mu}^g$ is its change upon geometry change; α_e is the electronic polarizability at the gas phase geometry $\mathbf{G}^g$; and $\Delta\alpha_e$ is its deformation-induced change.

We now assume for the liquid phase that $\Delta\alpha_e$ is mainly determined by the difference between $\mathbf{G}^g$ and the average geometry $\mathbf{G}^l$ in the liquid[42,43] and that the fluctuations of $\mathbf{G}(\langle \mathbf{E} \rangle_v)$ around $\mathbf{G}^l$ can be neglected. Furthermore, we assume that the deformation-induced change $\Delta\boldsymbol{\mu}^g$ of the dipole moment $\boldsymbol{\mu}^g$ obeys the linear response relation

$$\Delta\boldsymbol{\mu}^g = \alpha_G \langle \mathbf{E} \rangle_v \quad (2)$$

Then eq 1 reduces to

$$\boldsymbol{\mu} = \boldsymbol{\mu}^g + \alpha_{tot} \langle \mathbf{E} \rangle_v \quad (3)$$

with the total polarizability

$$\alpha_{tot} = \alpha_e + \Delta\alpha_e + \alpha_G \quad (4)$$

covering additionally those changes of the dipole moment and of the polarizability that are mediated in the liquid phase by field-induced alterations of the molecular geometry. Thus, we model the total polarizability α_{tot} of a water molecule in a liquid phase environment by three contributions. (i) The electronic contribution α_e measures the change of the dipole moment at the experimental gas phase geometry $\mathbf{G}^g$ upon exposure to the average reaction field $\langle \mathbf{E} \rangle_v$ in the liquid phase. (ii) $\Delta\alpha_e$ is the change of the electronic polarizability associated with the transition from $\mathbf{G}^g$ to $\mathbf{G}^l$. (iii) The deformation contribution α_G measures the change of the dipole moment caused by this transition.

We will check by DFT/MM-MD simulations at what accuracy the modified linear response eq 3 can account for the dipole moment of a quantum mechanically described and flexible water molecule embedded in a MM environment. Here, we will determine the geometry-dependent corrections $\Delta\alpha_e$ and α_G to the electronic polarizability α_e of the water molecule and will demonstrate that these corrections are small and happen to cancel quite precisely. This result modifies an earlier expectation of Smith et al.[44] who stated that the "effect of flexibility is greatest for dielectric properties, but in general it is found to be small" to the concise statement "the effect of flexibility vanishes for the dipole moment".

2. Methods

For our DFT and DFT/MM calculations of water molecules exposed to external electric fields, we employed the program packages CPMD[45] and EGO/CPMD,[15,37] respectively. CPMD is a grid-based DFT code that uses plane wave basis sets for the expansion of the Kohn−Sham orbitals and pseudopotentials to model the core electrons. We applied the gradient-corrected exchange functional of Becke,[46] the correlation functional of Perdew,[47] and the norm-conserving pseudopotentials of Troullier and Martins[48] to those water molecules, which represented the DFT fragments in our DFT/MM calculations. These DFT water molecules were enclosed into a cubic box of edge length 9 Å such that every atomic site was more than 3 Å distant from the faces of the box. The edges of the box were aligned with the coordinate axes shown in Figure 1. In CPMD, this box contains the grid for the plane wave basis set. The basis set was cutoff at 80 Ry. We denote this particular DFT approach by MT/BP.

2.1. Homogeneous Fields. To compute the components α_{ll}, $l \in \{x, y, z\}$ of the polarizability tensor $\boldsymbol{\alpha}$ for a water molecule,

we carried out a series of DFT calculations applying homogeneous fields $\mathbf{E}^{h}$ of varying directions and strengths. Here, we chose fields parallel to the axes l of the Cartesian coordinate system shown in Figure 1. For the field components E_l^h, we selected the range [−2 VÅ^{-1}, 2 VÅ^{-1}] because this range covers typical field strengths experienced by a water molecule in the bulk liquid at ambient temperature and pressure.[35] Choosing for each direction 19 equally spaced field values $E_{l,s}^h$ ($s = 1, ..., 19$) covering this range and keeping the molecule fixed at the optimal zero-field geometry $\hat{\mathbf{G}}^g \equiv \mathbf{G}(\mathbf{E}^h = 0)$, we calculated the dipole moments $\hat{\boldsymbol{\mu}}(E_{l,s}^h)$ induced by the external fields $E_{l,s}^h$.

These series of calculations yielded the polarizability tensor $\hat{\alpha}_{e,ll}^h$ through fitting seventh-order polynomials to the calculated dipole moments $\hat{\boldsymbol{\mu}}(E_{l,s}^h)$. At zero field, these fits reproduced the MT/BP prediction $\hat{\boldsymbol{\mu}}^g(\hat{\mathbf{G}}^g)$ for the dipole moment of an isolated water molecule, of course. Isotropic polarizabilities $\hat{\alpha}_e^h$ were then calculated by a global fit to the absolute values of the induced dipole moments $\hat{\boldsymbol{\mu}}^i(E_{l,s}^h) \equiv \hat{\boldsymbol{\mu}}(E_{l,s}^h) - \hat{\boldsymbol{\mu}}^g(\hat{\mathbf{G}}^g)$.

2.2. Geometry Dependence. In addition, we calculated how the dipole moment $\hat{\mu}^g$ and the electronic polarizability $\hat{\alpha}_e^h$ depend on the bond length r_{OH} and angle φ_{HOH} upon symmetric deformations of the equilibrium geometry $\hat{\mathbf{G}}^g$. For this purpose, we generated a set of different symmetric geometries $\mathbf{G}^s \equiv (r_{OH}, \varphi_{HOH})$ by varying the bond length r_{OH} within the range [0.94 Å, 1.04 Å] in steps of 0.01 Å and the angle φ_{HOH} within [90°, 118°] in steps of 2°. For each of these geometries $\mathbf{G}^s$, we calculated the dipole moment $\hat{\boldsymbol{\mu}}^g(\mathbf{G}^s)$ and the polarizability $\hat{\alpha}_{e,xx}^h(\mathbf{G}^s)$ by applying homogeneous fields along the bisectrix of the molecule. The chosen ranges of r_{OH} and φ_{HOH} cover the values observed in the DFT/MM simulations described below.

2.3. Flexible DFT Water Molecule in Liquid MM Water. Beyond the thus obtained insight into the response of a water molecule to homogeneous external fields, we also wanted to gain access to its response to the inhomogeneous fields acting in the liquid phase. Therefore we carried out several DFT/MM-MD simulations of a flexible DFT water molecule embedded in an MM liquid water environment.

Here, three periodic orthorhombic dodecahedra, each with an inner radius of 21.8 Å, were filled with 1970 TIP4P water models[5] and one additional TIP3P water model[5] that was designated for the subsequent DFT treatment. Using the EGO-MMII program package,[15] these systems were equilibrated for 1 ns by MM−MD in the *NpT* ensemble, i.e., at constant pressure p, temperature T, and number N of atoms. To keep the pressure at 1×10^5 Pa and the temperature at 293 K, we employed Berendsen thermo- and barostats[49] at coupling times of 10 ps (T) and 0.1 ns (p), respectively. Additionally, the barostat was parametrized with the isothermal compressibility of 4.6×10^{-10} Pa^{-1}, which is the experimental value for liquid water at the given conditions.[50] The long-range electrostatic interactions were treated by the structure-adapted fast multipole method[51] combined with a reaction field correction, i.e., by the SAMM/RF algorithm described in ref 15. The van der Waals interactions beyond a cutoff at 10 Å were treated in a mean field way. The water models were kept rigid by the M-SHAKE algorithm[52] with a relative tolerance of 10^{-6}. The Verlet algorithm[53] was applied to integrate the equations of motion with a time step of 1 fs.

After this MM−MD equilibration, the TIP3P model was replaced by a flexible MT/BP water model. The systems were equilibrated for an additional 15 ps by (MT/BP)/MM−MD using a time step of 0.25 fs. For this additional equilibration and the following calculations, the barostat was disabled (*NVT* ensemble), and the thermostat was restricted to the MM fragment.

TABLE 1: Geometries and Dipole Moments of the Water Molecule

method	r_{OH}/Å	φ_{HOH}/deg	geometry	μ_x/D
MT/BP	0.976	103.9	$\hat{\mathbf{G}}^g$	1.81
BLYP[a]	0.972	104.4	$\tilde{\mathbf{G}}^g$	1.87
gas phase[b]	0.957	104.5	$\mathbf{G}^g$	1.85
liquid phase[c]	0.968	105.3	$\mathbf{G}^l$	—
BLYP-MD[a]	0.992	105.5	$\langle\tilde{\mathbf{G}}^l\rangle$	∼2.97
(MT/BP)/MM−MD	0.986	103.4	$\langle\hat{\mathbf{G}}^l\rangle_T$	2.40

[a] From ref 9. [b] From refs 38 and 55. [c] From refs 42 and 43.

Following the equilibration, a total simulation time of 300 ps was spent to the three simulation systems giving rise to a combined trajectory **T**. At each femtosecond, the dipole moment $\boldsymbol{\mu}(t)$ and the geometry $\mathbf{G}(t)$ of the DFT fragment were noted for later analysis. In addition, the average electric reaction field $\langle\mathbf{E}\rangle_v$ within the volume v of the DFT water molecule was calculated as described in ref 35. Here, a value $\sigma = 0.725$ Å was chosen for the width of the Gaussian kernel approximating the molecular volume, because the polarizability calculated from the volume average field $\langle\mathbf{E}\rangle_v$ assumes at this width the value determined in homogeneous external fields (cf. Figure 4A of ref 35).

3. Results

As outlined in the Introduction, we want to analyze how strongly the liquid phase polarizability α_{tot} of a water molecule differs from the gas phase polarizability α_e. According to eq 4, this difference can be expressed through the contributions $\Delta\alpha_e$ and α_G, which arise from the geometry change $\Delta\mathbf{G}^{l,g}$ associated with the transfer into the liquid. To characterize this change, we first compare the experimental geometries $\mathbf{G}^g$ and $\mathbf{G}^l$ of a water molecule in the gas and liquid phase, respectively, with the corresponding MT/BP and (MT/BP)/MM−MD predictions $\hat{\mathbf{G}}^g$ and $\langle\hat{\mathbf{G}}^l\rangle_T$.

3.1. Geometry and Dipole Moment. The first line in Table 1 specifies the optimized geometry $\hat{\mathbf{G}}^g$ and the associated x-component $\hat{\mu}_x^g$ of the dipole moment resulting from our MT/BP description of an isolated water molecule (cf. the coordinate system in Figure 1). In the second line, these data are compared with a BLYP[46,54] description by Silvestrelli et al.[9] For comparison, the experimental gas phase data on the geometry $\mathbf{G}^g$ and dipole moment μ_x^g are listed immediately below. The remainder of the table describes the properties of the water molecule in the liquid.

Table 1 shows that the DFT functionals overestimate the gas phase bond length r_{OH}^g by 2.0% (MT/BP) and 1.6% (BLYP), respectively. The experimental bond angle φ_{HOH}^g is nearly reproduced by BLYP, whereas MT/BP yields a 0.6% underestimate. For the liquid phase, the table reveals similar deviations between the experimental geometry and the two theoretical descriptions. Here, the average bond lengths $\langle r_{OH}\rangle$ predicted by the MD simulations overestimate the experimental value r_{OH}^l by 1.9% [(MT/BP)/MM] and 2.5% (BLYP), respectively. Furthermore, the average bond angle $\langle\tilde{\varphi}_{HOH}\rangle$ resulting from BLYP−MD matches the experimental angle φ_{HOH}^l within 0.2%, whereas the average angle $\langle\hat{\varphi}_{HOH}\rangle_T$ predicted by our 300 ps (MT/BP)/MM−MD trajectory **T** is by 1.8% too small. Because the deviations between the predicted and measured geometries are similar for the two phases, they are most likely intrinsic properties of the respective DFT approaches.

Considering that MT/BP predicts for the gas phase a larger bond length and a smaller bond angle than experimentally

TABLE 2: Geometry Changes of a Water Molecule upon Gas−Liquid Transfer

source	Δr_{OH}/Å	$\Delta\varphi_{HOH}$/deg	geometry change
this work	0.010	−0.5	$\langle\Delta\hat{\mathbf{G}}^{l,g}\rangle_T \equiv \langle\hat{\mathbf{G}}^l\rangle_T - \hat{\mathbf{G}}^g$
ref 9	0.020	1.1	$\langle\Delta\tilde{\mathbf{G}}^{l,g}\rangle \equiv \langle\tilde{\mathbf{G}}^l\rangle - \tilde{\mathbf{G}}^g$
experiment[38,42,43]	0.011	0.8	$\Delta\mathbf{G}^{l,g} \equiv \mathbf{G}^l - \mathbf{G}^g$

TABLE 3: Gas Phase Polarizability of a Water Molecule

method		$\alpha^h_{e,xx}$/Å^3	$\alpha^h_{e,yy}$/Å^3	$\alpha^h_{e,zz}$/Å^3	α^h_e/Å^3
MT/BP	($\hat{\mathbf{G}}^g$)	1.62	1.63	1.60	1.62
experiment[36]	($\mathbf{G}^g$)	1.47	1.53	1.42	1.47

observed, one would naively expect that MT/BP should predict a dipole moment $\hat{\mu}^g_x(\hat{\mathbf{G}}^g)$ larger than the experimental value $|\boldsymbol{\mu}^g| = 1.85$ D. However, the MT/BP result is actually by 2.2% smaller. Also, the BLYP description slightly misses the experimental value and yields a 1.1% overestimate.

For the dipole moment of a water molecule in the liquid phase, one cannot give an accurate experimental reference. For this case, the two MD descriptions yield strongly different predictions. The average dipole moment $\langle\hat{\mu}^l_x\rangle_T = 2.40$ D predicted by our hybrid trajectory **T** is by about 0.6 D larger than the MT/BP vacuum value and close to the dipole moments of the most commonly used MM water models (TIP3P: 2.35 D, SPC/E: 2.35 D).[5,6] It is a little larger than the dipole moment (2.17 D) of the TIP4P potential[5] modeling the MM solvent in **T**. In contrast, the fully quantum mechanical BLYP−MD simulation predicts a much larger increase of about 1.1 D for the transfer into the liquid phase resulting in the very large average value $\langle\tilde{\mu}^l_x\rangle = 2.97$D.

3.2. Geometry Changes $\Delta\mathbf{G}^{l,g}$. At the beginning of section 3, we have emphasized that we want to identify the changes of the polarizability which are caused by the geometry changes $\Delta\mathbf{G}^{l,g}$ accompanying the transfer of a water molecule from the gas into the liquid phase. The changes $\Delta\mathbf{G}^{l,g}$ and their computational descriptions follow immediately from the data in Table 1 and are listed in Table 2.

According to Table 2, the experimental transfer-induced elongation $\Delta r^{l,g}_{OH}$ of the bond length is nicely reproduced by the average value $\langle\Delta\hat{r}^{l,g}_{OH}\rangle_T$ extracted from the hybrid trajectory **T** and the MT/BP vacuum calculation. In contrast, the BLYP−MD simulation overestimates $\Delta r^{l,g}_{OH}$ by a factor of 2. On the other hand, the latter simulation correctly predicts a widening of the bond angle, whereas (MT/BP)/MM−MD assigns a slight compression $\langle\Delta\hat{\varphi}^{l,g}_{OH}\rangle_T$ to this angle upon transfer. It will now be interesting to see how such geometry changes alter the polarizability of the water molecule.

Because our earlier work[35] has demonstrated for the liquid phase that the electric field within the volume v of a water molecule exhibits substantial inhomogeneities, we expect that the geometry-dependent modifications $\Delta\alpha_e$ and α_G will be influenced by these inhomogeneities. To enable an identification of the effects of inhomogeneity we first consider the equivalent quantities $\Delta\alpha^h_e$ and α^h_G for homogeneous electric fields.

3.3. Response of a Water Molecule to Homogeneous Fields. To characterize the response of a water molecule to homogeneous fields, we have first chosen the MT/BP vacuum geometry $\hat{\mathbf{G}}^g$ and have calculated the field dependence of the dipole moment by applying homogeneous fields of varying strengths. The polarizability tensor $\hat{\boldsymbol{\alpha}}^h_e(\hat{\mathbf{G}}^g)$ has been calculated from these data by the methods described in section 2.1.

Table 3 compares the MT/BP results with experimental data on the polarizability of a water molecule in the gas phase[36] and demonstrates that the predicted polarizability $\hat{\alpha}^h_e(\hat{\mathbf{G}}^g)$ overestimates the gas phase value α^{exp} by 10.2%. Furthermore, in mild contrast to the experimental data, the polarizability tensor $\hat{\boldsymbol{\alpha}}^h_e(\hat{\mathbf{G}}^g)$ is calculated to be nearly isotropic. According to the recent BLYP−MD study of Salanne et al.,[56] the near isotropy should also hold in the liquid phase. Therefore, and because according to the trajectory **T** the average polarizing field $\langle\langle\mathbf{E}\rangle_v\rangle_T$ is oriented along the bisectrix of the H_2O molecule, one may safely assume that in the liquid the polarizability $\alpha^l \equiv |\boldsymbol{\alpha}^l|$ is given by α^l_{xx} to a very good approximation. Consequently, we will identify these two quantities from now on.

Note here that the polarizability $\hat{\alpha}^h_e(\mathbf{G}^g)$, which has been determined in our earlier work[35] by the same MT/BP method but for a different geometry, i.e., the experimental gas phase geometry $\mathbf{G}^g$, was 2.5% smaller than $\hat{\alpha}^h_e(\hat{\mathbf{G}}^g)$. This difference indicates that the polarizability of a water molecule is affected by the geometry chosen for the computation.

3.3.1. Geometry Dependence of Properties. To elucidate this dependence, we have calculated (cf. section 2.2) the zero-field dipole moments $\hat{\mu}^g(\mathbf{G}^s)$ and the responses $\hat{\alpha}^h_e(\mathbf{G}^s)$ to homogeneous fields for several symmetric geometries $\mathbf{G}^s$ in a neighborhood of the average geometry $\langle\hat{\mathbf{G}}^l\rangle_T$ obtained from the trajectory **T** (cf. Table 1). The results are displayed by Figure 2 as contour plots of $\hat{\mu}^g(\mathbf{G}^s)$ and $\hat{\alpha}^h_e(\mathbf{G}^s)$ on the (r_{OH}, φ_{HOH})-plane.

Figure 2A demonstrates that the dipole moments $\hat{\mu}^g(\mathbf{G}^s)$ depend almost exclusively on the bond angle φ_{HOH}. Taking the dipole moment $\hat{\mu}^g(\hat{\mathbf{G}}^g)$ at the MT/BP vacuum geometry $\hat{\mathbf{G}}^g$ as the reference, this finding may be expressed by the approximate linear response relation for the geometry-dependent change

$$\Delta\hat{\mu}^g(\mathbf{G}^s) \simeq -\lambda^g_\varphi\Delta\varphi_{HOH} \tag{5}$$

of $\hat{\mu}^g$, where the response parameter λ^g_φ is 0.0145 D/deg and $\Delta\varphi_{HOH}$ is defined as $\varphi_{HOH} - \hat{\varphi}^g_{HOH}$.

According to Figure 2B, the electronic polarizability $\hat{\alpha}^h_e$ depends almost exclusively on the bond length r_{OH} at symmetric deformation. Also, this dependence can be quite accurately modeled by a linear response relation for the geometry-dependent change

$$\Delta\hat{\alpha}^h_e(\mathbf{G}^s) \simeq \beta^h_r\Delta r_{OH} \tag{6}$$

of the polarizability $\hat{\alpha}^h_e$ around its value at $\hat{\mathbf{G}}^g$. Here, the parameter $\beta^h_r = 2.08$ Å^2 quantifies the response, and $\Delta r_{OH} \equiv r_{OH} - \hat{r}^g_{OH}$. As a result of these response properties, $\hat{\mu}^g$ decreases by 0.8% for $\Delta\varphi_{HOH} = 1°$ and $\hat{\alpha}^h_e$ increases by 1.3% for $\Delta r_{OH} = 0.01$ Å.

3.3.2. Estimates for $\Delta\hat{\alpha}^T_e$, $\hat{\alpha}^T_G$, and $\hat{\alpha}^T_{tot}$. The above results on the response of a water molecule to homogeneous external fields immediately lead to a corresponding estimate $\Delta\hat{\alpha}^{h,T}_e$ specifying how much one has add to the MT/BP vacuum polarizability $\hat{\alpha}^h_e(\hat{\mathbf{G}}^g) = 1.62$ Å^3 (cf. Table 3) to obtain the electronic polarizability of the MT/BP water model embedded in the TIP4P solvent. Inserting the gas−liquid bond elongation $\langle\Delta\hat{r}^{l,g}_{OH}\rangle_T$ determined by our calculations (cf. Table 2) into eq 6 yields $\Delta\hat{\alpha}^{h,T}_e = 0.021$ Å^3 representing a 1.3% increase compared to $\hat{\alpha}^h_e(\hat{\mathbf{G}}^g)$.

In a similar way, the relatively strong dependence of the dipole moment $\hat{\mu}^g(\mathbf{G})$ on the bond angle φ_{HOH} can be utilized to estimate the deformation polarizability $\hat{\alpha}^{g,T}_G$, which is expected for a MT/BP water model in the TIP4P liquid. Inserting the narrowing $\langle\Delta\hat{\varphi}^{l,g}_{OH}\rangle_T = -0.5°$ of the bond angle (cf. Table 2) into eq 5 yields the geometry induced change $\Delta\hat{\mu}^g(\langle\hat{\mathbf{G}}^l\rangle_T) =$

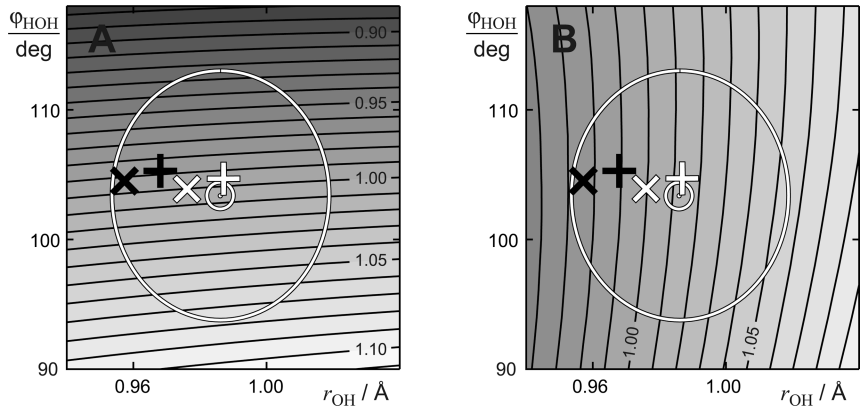

Figure 2. Relative (A) dipole moments $\hat{\mu}^{g}(\mathbf{G}^{s})/\hat{\mu}^{g}(\hat{\mathbf{G}}^{g})$ and (B) polarizabilities $\hat{\alpha}_{e}^{h}(\mathbf{G}^{s})/\hat{\alpha}_{e}^{h}(\hat{\mathbf{G}}^{g})$ calculated by MT/BP for symmetric water geometries $\mathbf{G}^{s}$. The white cross (×) marks the MT/BP vacuum geometry $\hat{\mathbf{G}}^{g}$ serving as the reference. The white ellipses are centered at the average geometry $\langle\hat{\mathbf{G}}^{l}\rangle_{T}$ (white circle) predicted by the trajectory **T** and limit 2σ environments, where $\sigma_{r/\varphi}$ are the standard deviations of the geometries $\mathbf{G}(t)$ sampled by **T**. The white plus sign (+) specifies a hypothetical liquid phase geometry $\hat{\mathbf{G}}^{l} = \hat{\mathbf{G}}^{g} + \Delta\mathbf{G}^{l,g}$, where $\Delta\mathbf{G}^{l,g}$ is the experimental geometry change (cf. Table 2). The experimental geometries are indicated by black symbols ($\mathbf{G}^{g}$, ×; $\mathbf{G}^{l}$, +).

0.007 D. If we adopt for the liquid phase the average electric field $\langle\langle E_x\rangle_v\rangle_T = 1.03$ VÅ^{-1} resulting from our trajectory **T** and employ eq 2, we find the homogeneous field estimate for the deformation polarizability

$$\hat{\alpha}_{G}^{h,T} = \frac{\Delta\hat{\mu}^{g}(\langle\hat{\mathbf{G}}^{l}\rangle_{T})}{\langle\langle E_x\rangle_v\rangle_T} = 0.021\ \text{Å}^3$$

With eq 4 and with the electronic polarizability $\hat{\alpha}_{e}^{h} = 1.62$ Å^3 obtained by MT/BP at the vacuum geometry $\hat{\mathbf{G}}^{g}$ (cf. Table 3), the above estimates for $\Delta\hat{\alpha}_{e}^{h,T}$ and $\hat{\alpha}_{G}^{g,T}$ immediately yield the first guess $\hat{\alpha}_{tot}^{h,T} = 1.66$ Å^3 for the total polarizability. This estimate relies on the assumption that a water molecule in the liquid is exposed to to homogeneous external fields. Because this assumption is definitely violated,[35] we will now check our estimate by analyzing the trajectory **T**.

3.4. Response of a Water Molecule in the Liquid. Within the MD trajectory **T**, the geometry $\mathbf{G}(t)$ of the MT/BP water molecule fluctuates around the average geometry $\langle\hat{\mathbf{G}}^{l}\rangle_{T}$. According to eq 3, the induced dipole moments $\boldsymbol{\mu}^{i}(t) \equiv \boldsymbol{\mu}(t) - \hat{\boldsymbol{\mu}}^{g}(\hat{\mathbf{G}}^{g})$ should depend, on the average, linearly on the electric field $\langle\mathbf{E}\rangle_v(t)$ within the water molecule with a linear response parameter α_{tot}^{T} defining the total polarizability.

Figure 3 verifies this expectation. It shows that the data points $(|\boldsymbol{\mu}^{i}(t)|,|\langle\mathbf{E}\rangle_v(t)|)$ contained in **T** are approximately described by a linear regression, whose slope is the (MT/BP)/MM−MD prediction for total polarizability $\alpha_{tot}^{T} = 1.68$ Å^3 of a flexible DFT water model in a TIP4P environment. This value is larger than our above estimate $\hat{\alpha}_{tot}^{h,T} = 1.66$ Å^3 and much larger than the MT/BP vacuum value $\alpha_{e}^{h} = 1.62$ Å^3 (cf. Table 3). Interestingly, the value also differs from the previous (MT/BP)/MM−MD result (1.58 Å^3) obtained for a DFT water model rigidly fixed at the experimental gas phase geometry $\mathbf{G}^{g}$. In the latter case, the polarizability derived from the correlation $|\boldsymbol{\mu}^{i}(|\langle\mathbf{E}\rangle_v|)|$ was identical to the gas phase polarizability.[35]

The data points in Figure 3 scatter around the regression line with an average deviation of 0.08 D. A comparison with the deviation of 0.02 D resulting for rigid water models[35] suggests that the additional broadening of 0.06 D should be due to the fluctuations of r_{OH} and φ_{HOH} around their average values. Because these fluctuations are documented in the MD trajectory, we can check this hypothesis by first deriving liquid phase analogues to the linear geometry response relations eqs 5 and 6.

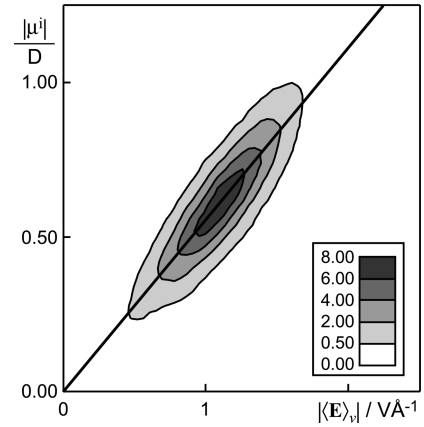

Figure 3. Correlations between the volume average electric fields $|\langle\mathbf{E}\rangle_v|$ and the induced dipole moments $|\boldsymbol{\mu}^{i}|$ in the DFT/MM trajectory **T**. The histogram shows the frequency of data pairs $(|\boldsymbol{\mu}^{i}|, |\langle\mathbf{E}\rangle_v|)$ in units of Å(VD)$^{-1}$. The black line is the linear regression subject to the constraint $|\boldsymbol{\mu}^{i}| = 0$ for $|\langle\mathbf{E}\rangle_v| = 0$.

3.4.1. Geometry Dependence of $\Delta\alpha_e$ and α_G Derived from T. To determine the liquid phase response parameters β_r^{T} and λ_φ^{T} from the dipole moments $\boldsymbol{\mu}(t)$ and symmetrized geometries $\mathbf{G}^{s}(t)$ collected in the trajectory **T**, we consider eq 1. Assuming that eqs 5 and 6 also hold in the liquid phase and inserting these equations into eq 1 yield the approximate prediction

$$\hat{\mu}_x(\mathbf{G}^{s}) = \hat{\mu}_x^{g}(\hat{\mathbf{G}}^{g}) - \lambda_\varphi^{T}(\delta\varphi_{HOH} + \langle\Delta\hat{\varphi}_{OH}^{l,g}\rangle_T) + [\alpha_e^{h} + \beta_r^{T}(\delta r_{OH} + \langle\Delta\hat{r}_{OH}^{l,g}\rangle_T)]\langle E_x\rangle_v \quad (7)$$

for the x-component of the dipole moment. Here, we have used the average geometry changes $\langle\Delta\hat{\mathbf{G}}^{l,g}\rangle_T = (\langle\Delta\hat{r}_{OH}^{l,g}\rangle_T, \langle\Delta\hat{\varphi}_{OH}^{l,g}\rangle_T)$, which are given in the first line of Table 2 and belong to the transfer of the MT/BP water model from the vacuum into the TIP4P liquid. Additionally, we have introduced the dynamical fluctuations of the symmetrized bond lengths $\delta r_{OH} \equiv (r_{OH,1} + r_{OH,2})/2 - \langle\hat{r}_{OH}^{l}\rangle_T$ and of the bond angles $\delta\varphi_{HOH} \equiv \varphi_{HOH} - \langle\hat{\varphi}_{HOH}^{l}\rangle_T$ around the average liquid phase geometry $\langle\hat{\mathbf{G}}^{l}\rangle_T$. Furthermore, $\hat{\alpha}_e^{h} = 1.62$ Å^3 is the electronic polarizability of an MT/BP water model at the optimized vacuum geometry $\hat{\mathbf{G}}^{g}$.

According to eqs 2, 4, 5, and 6, the total polarizability, which measures the slope of the linear regression in Figure 3, should be given by

$$\hat{\alpha}^{\mathrm{T}}_{\mathrm{tot}} = \hat{\alpha}^{\mathrm{h}}_{\mathrm{e}} + \beta^{\mathrm{T}}_{r}\langle\Delta\hat{\varphi}^{\mathrm{l,g}}_{\mathrm{OH}}\rangle_{\mathrm{T}} - \lambda^{\mathrm{T}}_{\varphi}\langle\Delta\hat{\varphi}^{\mathrm{l,g}}_{\mathrm{OH}}\rangle_{\mathrm{T}}/\langle\langle E_x\rangle_v\rangle_{\mathrm{T}}, \quad (8)$$

where $\langle\langle E_x\rangle_v\rangle_{\mathrm{T}} = 1.03\ \mathrm{V\AA^{-1}}$ is the trajectory average of the volume average field $\langle E_x\rangle_v$. With the estimated induced dipole moment $\hat{\mu}^{\mathrm{i}}_x(\mathbf{G}^{\mathrm{s}}) \equiv \hat{\mu}_x(\mathbf{G}^{\mathrm{s}}) - \hat{\mu}^{\mathrm{g}}_x(\hat{\mathbf{G}}^{\mathrm{g}})$, eq 7 then reduces to

$$\hat{\mu}^{\mathrm{i}}_x(\mathbf{G}^{\mathrm{s}}) = \hat{\alpha}^{\mathrm{T}}_{\mathrm{tot}}\langle E_x\rangle_v - \lambda^{\mathrm{T}}_{\varphi}\delta\varphi_{\mathrm{HOH}} + \beta^{\mathrm{T}}_{r}\delta r_{\mathrm{OH}}\langle E_x\rangle_v \quad (9)$$

If one adopts for the total polarizability $\hat{\alpha}^{\mathrm{T}}_{\mathrm{tot}}$ the value $\alpha^{\mathrm{T}}_{\mathrm{tot}} = 1.68\ \mathrm{\AA^3}$ determined from the linear regression in Figure 3, then the first term on the right-hand side of eq 9 represents the regression line. The remaining terms predict the field- and geometry-dependent fluctuations of the induced dipole moments around the regression line.

The parameters β^{T}_r and $\lambda^{\mathrm{T}}_{\varphi}$ in eq 9 can now be determined by minimizing the root-mean-square difference between the (MT/BP)/MM−MD results $\mu^{\mathrm{i}}_x(t)$ and the values $\hat{\mu}^{\mathrm{i}}_x(t)$, which are predicted by eq 9 from the symmetrized geometries $\mathbf{G}^{\mathrm{s}}(t)$ and volume average fields $\langle E_x\rangle_v(t)$ collected in $\mathbf{T}$. By an iterative minimization procedure, we obtained the values $\beta^{\mathrm{T}}_r = 3.80\ \mathrm{\AA^2}$ and $\lambda^{\mathrm{T}}_{\varphi} = 0.0161$ D/deg. Both parameters are larger than their counterparts β^{h}_r and $\lambda^{\mathrm{g}}_{\varphi}$ determined in section 3.3.1 for homogeneous environments.

3.4.2. Polarizability at $\langle\hat{\mathbf{G}}^{\mathrm{l}}\rangle_{\mathrm{T}}$. Inserting now the above values for β^{T}_r and $\lambda^{\mathrm{T}}_{\varphi}$ together with the geometry change $\langle\Delta\hat{\mathbf{G}}^{\mathrm{l,g}}\rangle_{\mathrm{T}}$ (cf. Table 2) into eq 8 yields the (MT/BP)/MM−MD prediction $\hat{\alpha}^{\mathrm{T}}_{\mathrm{tot}} = 1.68\ \mathrm{\AA^3}$ for the total polarizability of a water molecule at $\langle\hat{\mathbf{G}}^{\mathrm{l}}\rangle_{\mathrm{T}}$. $\hat{\alpha}^{\mathrm{T}}_{\mathrm{tot}}$ is equal to the value $\alpha^{\mathrm{T}}_{\mathrm{tot}}$ giving the slope of the linear regression in Figure 3. However, as is apparent from a comparison with eqs 5 and 6, eq 8 additionally yields the (MT/BP)/MM−MD values $\Delta\hat{\alpha}^{\mathrm{T}}_{\mathrm{e}} = 0.038\ \mathrm{\AA^3}$ and $\hat{\alpha}^{\mathrm{T}}_{\mathrm{G}} = 0.023\ \mathrm{\AA^3}$ for the geometry-dependent contributions to $\hat{\alpha}^{\mathrm{T}}_{\mathrm{tot}}$. These contributions explain the difference between $\hat{\alpha}^{\mathrm{T}}_{\mathrm{tot}} = 1.68\ \mathrm{\AA^3}$ and the electronic polarizability $\hat{\alpha}^{\mathrm{h}}_{\mathrm{e}} = 1.62\ \mathrm{\AA^3}$ of an isolated MT/BP water model fixed at the geometry $\hat{\mathbf{G}}^{\mathrm{g}}$.

If one compares the above results with the homogeneous field estimates $\Delta\hat{\alpha}^{\mathrm{h,T}}_{\mathrm{e}} = 0.021\ \mathrm{\AA^3}$ and $\hat{\alpha}^{\mathrm{h,T}}_{\mathrm{G}} = 0.021\ \mathrm{\AA^3}$ from section 3.3.2, one realizes that the angle dependence expressed by $\hat{\alpha}^{\mathrm{T}}_{\mathrm{G}}$ is largely unaffected by the field inhomogeneity, whereas the bond length dependence expressed by $\Delta\hat{\alpha}^{\mathrm{h,T}}_{\mathrm{e}}$ becomes more pronounced in the liquid.

The quality by which eq 9 can now predict the induced dipole moments $\mu^{\mathrm{i}}_x(t)$ contained in the trajectory $\mathbf{T}$ from the volume average fields $\langle\mathbf{E}\rangle_v(t)$ and geometries $\mathbf{G}^{\mathrm{s}}(t)$ is illustrated by Figure 4. The figure shows the correlation between the $\mu^{\mathrm{i}}_x(t)$ and the corresponding predictions $\hat{\mu}^{\mathrm{i}}_x(t)$, which were calculated by eq 9 with the optimized geometry response parameters β^{T}_r and $\lambda^{\mathrm{T}}_{\varphi}$. The average deviation is 0.03 D and, thus, is much smaller than the deviation of 0.08 D applying to the data in Figure 3. The strongly reduced scatter demonstrates that our simple model eq 9 for the geometry- and field-dependent contributions to the dipole moment holds to a very good approximation.

The small scatter in Figure 4 additionally demonstrates that eq 8 can not only predict the liquid phase polarizability $\alpha^{\mathrm{T}}_{\mathrm{tot}}$ at the average geometry $\langle\hat{\mathbf{G}}^{\mathrm{l}}\rangle_{\mathrm{T}}$ but can also accurately predict the polarizability at all geometries $\mathbf{G}^{\mathrm{s}}$ in the vicinity of $\langle\hat{\mathbf{G}}^{\mathrm{l}}\rangle_{\mathrm{T}}$. In particular, one can use eq 8 to compute the total polarizability $\hat{\alpha}^{\mathrm{l}}_{\mathrm{tot}}$ for the experimental geometry change $\Delta\mathbf{G}^{\mathrm{l,g}}$, which shifts $\mathbf{G}^{\mathrm{s}}$ from the optimized vacuum geometry $\hat{\mathbf{G}}^{\mathrm{g}}$ (white cross in Figure 2) to a hypothetical liquid phase geometry $\hat{\mathbf{G}}^{\mathrm{l}}$ (white plus sign in Figure 2). The polarizability $\hat{\alpha}^{\mathrm{l}}_{\mathrm{tot}}$ should represent a much better estimate for the experimental liquid phase polarizability

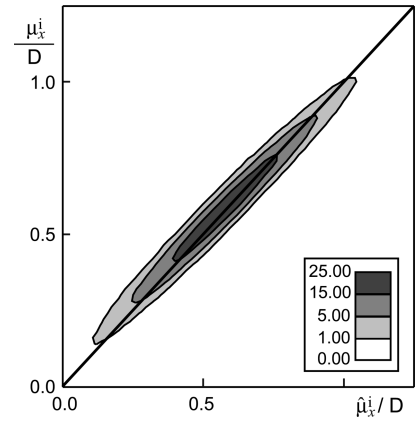

Figure 4. Correlation between the induced (MT/BP)/MM−MD dipole moments $\mu^{\mathrm{i}}_x(t)$ and the predictions $\hat{\mu}^{\mathrm{i}}_x(t)$ according to eq 9. The data are shown as a histogram in units of $\mathrm{D^{-2}}$ representing a normalized estimate for the probability density. The black line is the bisectrix of the coordinate system.

than the value $\hat{\alpha}^{\mathrm{T}}_{\mathrm{tot}}$ obtained for $\langle\hat{\mathbf{G}}^{\mathrm{l}}\rangle_{\mathrm{T}}$ because the experimental geometry change $\Delta\mathbf{G}^{\mathrm{l,g}}$ is poorly described by $\langle\Delta\hat{\mathbf{G}}^{\mathrm{l,g}}\rangle_{\mathrm{T}}$ (cf. Table 2).

3.5. Polarizability Change upon $\Delta\mathbf{G}^{\mathrm{l,g}}$. Inserting $\Delta\mathbf{G}^{\mathrm{l,g}}$ into eq 8 yields a total liquid phase polarizability $\hat{\alpha}^{\mathrm{l}}_{\mathrm{tot}} = 1.62$, which happens to be identical to the value predicted by MT/BP for the H_2O molecule in the vacuum. The invariance of the polarizability, which thus follows from our calculations for the transfer into the liquid phase assuming the experimental geometry change $\Delta\mathbf{G}^{\mathrm{l,g}}$, is caused by the cancellation of two contributions. On one hand, the bond elongation $\Delta r^{\mathrm{l,g}}_{\mathrm{OH}}$ leads to an increase $\Delta\hat{\alpha}^{\mathrm{l}}_{\mathrm{e}} = \beta^{\mathrm{l}}_r\Delta r^{\mathrm{l,g}}_{\mathrm{OH}} = 0.042\ \mathrm{\AA^3}$ of the electronic polarizability. On the other hand, the widening $\Delta\varphi^{\mathrm{l,g}}_{\mathrm{OH}}$ of the bond angle leads to a negative deformation polarizability $\hat{\alpha}^{\mathrm{l}}_{\mathrm{G}} = -\lambda^{\mathrm{T}}_{\varphi}\Delta\varphi^{\mathrm{l,g}}_{\mathrm{OH}}/\langle\langle E_x\rangle_v\rangle_{\mathrm{T}} = -0.038\ \mathrm{\AA^3}$. The total geometry-dependent variation $\Delta\hat{\alpha}^{\mathrm{l}}_{\mathrm{tot}} = \Delta\hat{\alpha}^{\mathrm{l}}_{\mathrm{e}} + \hat{\alpha}^{\mathrm{l}}_{\mathrm{G}} = 0.004$ D is then smaller than the numerical accuracy by which we have specified polarizabilities.

As a result, we see that the 3.6% increase of the total polarizability originally derived from the trajectory $\mathbf{T}$ is entirely due to the ill-description of the geometry change $\Delta\mathbf{G}^{\mathrm{l,g}}$ by the computational result $\langle\Delta\hat{\mathbf{G}}^{\mathrm{l,g}}\rangle_{\mathrm{T}}$. In particular, the erroneously predicted compression $\langle\Delta\hat{\varphi}^{\mathrm{l,g}}_{\mathrm{OH}}\rangle_{\mathrm{T}}$ of the bond angle is responsible for the difference between the small increase and the actual invariance.

Note here that the stated exact invariance of the polarizability upon transfer from the gas phase into the bulk liquid applies only to pure water. If ions or protein material are added to the solvent, then the geometries of the water molecules in the respective solvation shells may differ from the geometry in the pure liquid. However, due to the stiffness of the water molecules, these changes will be small, modifying the bond angle φ_{HOH} by at most a few degrees and the bond lengths r_{OH} by at most a few percent of an Ångstrøm. Then, according to our results, the changes of the polarizability will not exceed a few percent. Therefore, a polarizable water model suitable for the bulk liquid will show a reasonable performance also in heterogeneous systems.

4. Conclusion

For the construction of rigid, transferable, and point-polarizable MM water models, the above results limit the range of parameter choices. Such models should exhibit a dipole moment equal to the experimental gas phase value $\mu^{\mathrm{g}} = 1.85$ D. The geometry should be chosen such a way that the higher multipole

moments are optimally described within a given class of model complexity (the latter issue may require additional studies). For the polarizability, one should choose the experimental gas phase value $\alpha^{exp} = 1.47$ Å^3. However, because one does not have access to the volume average field $\langle \mathbf{E} \rangle_v$ in MM−MD simulations but has to use a spot check $\mathbf{E}(\mathbf{r}_\mu)$ instead, one must scale this field appropriately to account for the strong inhomogeneity of the electric field within the volume of a water molecule in a liquid surrounding.

If one takes the field $\mathbf{E}_O$ at the oxygen as a measure for $\langle \mathbf{E} \rangle_v$, then the optimal scaling factor is 0.684 as shown previously[35] and amounts to the use of an effective polarizability $\alpha^{eff} = 1.005$ Å^3. A corresponding stiff and point-polarizable MM water model will then automatically cover the geometry-dependent modifications of the polarizability, which are induced by the transfer from the gas into the liquid phase. Here, the slightly increased electronic polarizability that is caused by the bond elongation is exactly compensated by the small decrease of the dipole moment that is due to the widening of the bond angle.

Acknowledgment. This work was supported by the Deutsche Forschungsgemeinschaft (SFB 749/C4).

References and Notes

(1) Warshel, A.; Levitt, M. *J. Mol. Biol.* **1976**, *103*, 227–249.
(2) Tavan, P.; Carstens, H.; Mathias, G. Molecular dynamics simulations of proteins and peptides: Problems, achievements, and perspectives. In *Protein Folding Handbook*; Buchner, J., Kiefhaber, T., Eds.; Wiley-VCH: Weinheim, 2005; Vol. 1.
(3) Still, W. C.; Tempczyk, A.; Hawley, R. C.; Hendrickson, T. *J. Am. Chem. Soc.* **1990**, *112*, 6127–6129.
(4) Stork, M.; Tavan, P. *J. Chem. Phys.* **2007**, *126*, 165106.
(5) Jorgensen, W. L.; Chandrasekhar, J.; Madura, J. D.; Impey, R. W.; Klein, M. L. *J. Chem. Phys.* **1983**, *79*, 926–935.
(6) Berendsen, H. J. C.; Grigera, J. R.; Straatsma, T. P. *J. Phys. Chem.* **1987**, *91*, 6269–6271.
(7) Fanourgakis, G. S.; Xantheas, S. S. *J. Chem. Phys.* **2008**, *128*, 074506.
(8) Burnham, C. J.; Anick, D. J.; Mankoo, P. K.; Reiter, G. F. *J. Chem. Phys.* **2008**, *128*, 154519.
(9) Silvestrelli, P. L.; Parrinello, M. *J. Chem. Phys.* **1999**, *111*, 3572–3580.
(10) Guidon, M.; Schiffmann, F.; Hutter, J.; VandeVondele, J. *J. Chem. Phys.* **2008**, *128*, 214104.
(11) Zhou, R. H.; Berne, B. J. *Proc. Natl. Acad. Sci. U.S.A.* **2002**, *99*, 12777–12782.
(12) Zhou, R. H. *Proteins* **2003**, *53*, 148–161.
(13) Wroblewska, L.; Skolnick, J. *J. Comput. Chem.* **2007**, *28*, 2059–2066.
(14) Wang, J.; Cai, Q.; Li, Z.-L.; Zhao, H.-K.; Luo, R. *Chem. Phys. Lett.* **2009**, *468*, 112–118.
(15) Mathias, G.; Egwolf, B.; Nonella, M.; Tavan, P. *J. Chem. Phys.* **2003**, *118*, 10847–10860.
(16) Freddolino, P. L.; Liu, F.; Gruebele, M.; Schulten, K. *Biophys. J.* **2008**, *94*, L75–L77.
(17) Babitzki, G.; Denschlag, R.; Tavan, P. *J. Chem. Phys. B* **2009**, *113*, 10496–10508.
(18) Lopes, P. E. M.; Roux, B.; MacKerrel, A. D. *Theor. Chem. Acc.* **2009**, *124*, 11–28.
(19) Cieplak, P.; Dupradeau, F.-Y.; Duan, Y.; Wang, J. *J. Phys.: Condens. Matter* **2009**, *21*, 333402.
(20) Warshel, A.; Kato, M.; Pisliakov, A. V. *J. Chem. Theory Comput.* **2007**, *3*, 2034–2045.
(21) Caldwell, J.; Dang, L. X.; Kollman, P. A. *J. Am. Chem. Soc.* **1990**, *112*, 9144–9147.
(22) Kozack, R. E.; Jordan, P. C. *J. Chem. Phys.* **1991**, *96*, 3120–3130.
(23) Brodholt, J.; Sampoli, M.; Vallauri, R. *Mol. Phys.* **1995**, *86*, 149–158.
(24) Chialvo, A. A.; Cummings, P. T. *J. Chem. Phys.* **1996**, *105*, 8274–8281.
(25) Dang, L. X.; Chang, T.-M. *J. Chem. Phys.* **1997**, *106*, 8149–8159.
(26) Burnham, C. J.; Li, J.; Xantheas, S. S.; Leslie, M. *J. Chem. Phys.* **1999**, *110*, 4566–4581.
(27) Ren, P.; Ponder, J. W. *J. Phys. Chem.* **2003**, *107*, 5933–5947.
(28) Paricaud, P.; Předota, M.; Chivalvo, A. A.; Cummings, P. T. *J. Chem. Phys.* **2005**, *122*, 244511.
(29) Straatsma, T. P.; McCammon, J. A. *Chem. Phys. Lett.* **1990**, *167*, 252–254.
(30) Yu, H.; Hansson, T.; van Gunsteren, W. F. *J. Chem. Phys.* **2002**, *118*, 221–234.
(31) Yu, H.; van Gunsteren, W. F. *J. Chem. Phys.* **2004**, *121*, 9549–9564.
(32) Lamoureux, G.; MacKerell, A. D.; Roux, B. *J. Chem. Phys.* **2003**, *119*, 5185–5197.
(33) Lamoureux, G.; Harder, E.; Vorobyov, I. V.; Roux, B.; MacKerell, A. D. *Chem. Phys. Lett.* **2006**, *418*, 245–249.
(34) Kunz, A.-P. E.; van Gunsteren, W. F. *J. Phys. Chem. A* **2009**, *113*, 11570–11579.
(35) Schropp, B.; Tavan, P. *J. Phys. Chem. B* **2008**, *112*, 6233–6240.
(36) Murphy, W. F. *J. Chem. Phys.* **1977**, *67*, 5877–5882.
(37) Eichinger, M.; Tavan, P.; Hutter, J.; Parrinello, M. *J. Chem. Phys.* **1999**, *110*, 10452–10467.
(38) Benedict, W. S.; Gailar, N.; Plyler, E. K. *J. Chem. Phys.* **1956**, *24*, 1139–1165.
(39) Zhou, J.; Reich, S.; Brooks, B. R. *J. Chem. Phys.* **2000**, *112*, 7919–7929.
(40) Hess, B.; Saint-Martin, H.; Berendsen, H. J. C. *J. Chem. Phys.* **2002**, *116*, 9602–9610.
(41) Saint-Martin, H.; Hernández-Cobos, J.; Ortega-Blake, I. *J. Chem. Phys.* **2005**, *122*, 224509.
(42) Ichikawa, K.; Kameda, Y.; Yamaguchi, T.; Wakita, H.; Misawa, M. *Mol. Phys.* **1991**, *73*, 79–86.
(43) Thiessen, W. E.; Narten, A. H. *J. Chem. Phys.* **1982**, *77*, 2656–2662.
(44) Smith, D. E.; Haymet, A. D. J. *J. Chem. Phys.* **1992**, *96*, 8450–8459.
(45) CPMD V3.9 Copyright IBM Corp 1990−2004, Copyright MPI für Festkörperforschung Stuttgart 1997−2001, see also www.cpmd.org.
(46) Becke, A. D. *Phys. Rev. A* **1988**, *38*, 3098–3100.
(47) Perdew, J. P.; Yue, W. *Phys. Rev. B* **1986**, *33*, 8800–8802.
(48) Troullier, N.; Martins, J. L. *Phys. Rev. B* **1991**, *43*, 1993–2005.
(49) Berendsen, H. J. C.; Postma, J. P. M.; van Gunsteren, W. F.; DiNola, A.; Haak, J. R. *J. Chem. Phys.* **1984**, *81*, 3684–3690.
(50) Eisenberg, D.; Kauzmann, W. *The structure and properties of water*; Clarendon Press: Oxford, 1969.
(51) Niedermeier, C.; Tavan, P. *J. Chem. Phys.* **1994**, *101*, 734–748.
(52) Kräutler, V.; van Gunsteren, W. F.; Hünenberger, P. *J. Comput. Chem.* **2001**, *22*, 501–508.
(53) Verlet, L. *Phys. Rev.* **1967**, *159*, 98–103.
(54) Lee, C.; Yang, W.; Parr, R. G. *Phys. Rev. B* **1988**, *37*, 785–789.
(55) Clough, S. A.; Beers, Y.; Klein, G. P.; Rothman, L. S. *J. Chem. Phys.* **1973**, *59*, 2254–2259.
(56) Salanne, M.; Vuilleumier, R.; Madden, P. A.; Simon, C.; Turq, P.; Guillot, B. *J. Phys.: Condens. Matter* **2008**, *20*, 494207.

JP910932B